

Near-Field Integrated Sensing and Communications

Zhaolin Wang, *Graduate Student Member, IEEE*, Xidong Mu, *Member, IEEE*,
and Yuanwei Liu, *Senior Member, IEEE*

Abstract

A near-field integrated sensing and communications (NF-ISAC) framework is proposed, where both a sensing target and multiple communication users are located within the near-field region. An extended multiple signal classification (MUSIC) algorithm is proposed for the *joint distance and angle estimation*. The performance tradeoff between communication and sensing is characterized by the proposed two-stage algorithm. Numerical results reveal 1) the additional advantage of the NF-ISAC in terms of distance estimation compared to the conventional far-field ISAC, and 2) the tradeoff between the distance and angle estimation.

Index Terms

Integrated sensing and communications (ISAC), joint distance and angle estimation, near-field.

I. INTRODUCTION

The sixth-generation (6G) wireless network is envisioned to not only provide high-quality communication but also enable high-quality wireless sensing, thus supporting various emerging application scenarios from smart cities to smart homes. To this end, integrated sensing and communications (ISAC) has been regarded as a promising technique for 6G, where the sensing function and the communication function can be carried out simultaneously by sharing the same spectrum and hardware facilities [1], [2]. Therefore, there have been many works devoted to investigating ISAC systems recently [3]–[5].

To fulfill the increasing demand for communication and sensing performance, future ISAC systems will evolve towards large-antenna arrays and high-frequency bands, which are essential

for high communication capacity and high sensing resolution [2]. Nevertheless, such a trend will significantly change the electromagnetic properties of the wireless environment, i.e., from plane wave propagation to spherical wave propagation, leading to an inevitable near-field effect [6]. Thus, there can be a mismatch between existing ISAC designs relying on the far-field assumption [3]–[5] and real wireless environments, which requires a redesign of ISAC systems. Furthermore, the near-field effect also provides new possibilities. In particular, in conventional far-field ISAC systems, the angle and distance of the target are typically estimated based on the target response matrix (TRM) and the time delay of the signal, respectively [1]. Nevertheless, the time delay resolution can be limited by the system bandwidth and synchronization. When turning to the near-field region, the new distance dimension encapsulated in the spherical wave makes it possible for the joint distance and angle estimation without estimating time delay. However, to the best of the authors' knowledge, near-field ISAC (NF-ISAC) systems have not been studied yet, which motivates this work.

In this letter, we proposed a NF-ISAC framework. Based on the spherical wave propagation, we establish the accurate near-field channel model of the NF-ISAC framework. Then, for target sensing, we propose an extended multiple signal classification (MUSIC) algorithm for the joint distance and angle estimation, whose performance is characterized by the Cramér-Rao bound (CRB). Based on the proposed framework, we formulate a joint optimization problem to address the performance tradeoff between communication and sensing, which is solved by a two-stage algorithm. Our numerical results verify the effectiveness of the proposed framework.

II. SYSTEM MODEL

We consider a narrowband NF-ISAC system with a dual-functional BS equipped with N_t transmit antennas and N_r receive antennas. To enhance the energy efficiency, the hybrid beamforming (HB) structure is exploited at the BS, where the transmit and receive antennas are both connected to N_{RF} via analog phase shifters. The BS serves K single-antenna communication users, whose indices are in \mathcal{K} , and detects a single sensing target simultaneously. Both communication users and the sensing target are located in the near-field region with respect to the BS. In this work, we consider a coherent time block of length T , during which the communication channels and sensing target parameters remain approximately constant.

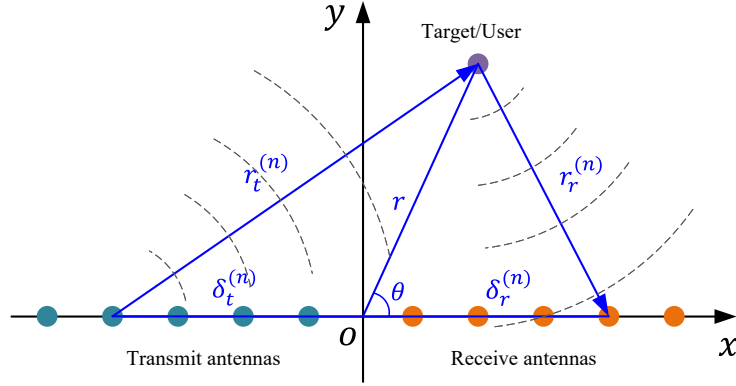


Fig. 1: Illustration of the near-field channel model based on the spherical wave.

A. Near-field Channel Model

In contrast to the far-field channel model where the signal wavefront is approximated to be plane, the near-field channel is modeled accounting for the accurate spherical wavefront. To evaluate the potential of the near-field model for communication and sensing, we consider the antenna setup at the BS as shown in Fig. 1. In particular, the transmit antenna array and the receive antenna array are assumed to be uniform linear arrays (ULAs), which are deployed adjacent to each other with a spacing of $2D$. The antenna spacing of the two antenna arrays is denoted as d .

Consider a point-like sensing target or communication user at the distance r and the angle θ with respect to the center of the two antenna arrays and take the transmit antenna array as an example. Based on the geometric relationship as shown in Fig. 1, the distance between the target/user and the n -element of the transmit antenna array is given by

$$\begin{aligned} r_t^{(n)}(r, \theta) &= \sqrt{r^2 + (\delta_t^{(n)})^2 - 2r\delta_t^{(n)} \cos \theta} \\ &\stackrel{(a)}{\approx} r - \delta_r^{(n)} \cos \theta + \frac{(\delta_r^{(n)})^2}{2r}, \end{aligned} \quad (1)$$

where $\delta_t^{(n)} = -nd - D$ denotes the distance between the centroid and the n -th element of the receive antenna array and the approximation (a) is obtained based on the first-order Taylor expansion $\sqrt{1+x} = 1 + \frac{1}{2}x + \mathcal{O}(x^2)$. Given the distance $r_t^{(n)}(r, \theta)$, the n -th element of the corresponding near-field beam focusing vector $\mathbf{a}_t(r, \theta) \in \mathbb{C}^{N_t \times 1}$ can be modeled as [7]

$$[\mathbf{a}_t(r, \theta)]_n = e^{-j\frac{2\pi}{\lambda}(r_t^{(n)}(r, \theta) - r)} = e^{-j\frac{2\pi}{\lambda}\left(-\delta_t^{(n)} \cos \theta + \frac{(\delta_t^{(n)})^2}{2r}\right)}. \quad (2)$$

The near-field beam focusing vector $\mathbf{a}_r(r, \theta) \in \mathbb{C}^{N_t \times 1}$ for the receive antenna array can be modeled in a similar way.

According to the above near-field beam focusing vectors, the communication channel $\mathbf{h}_k \in \mathbb{C}^{N_t \times 1}$ between the BS and the user k can be modeled as

$$\mathbf{h}_k = \alpha_k \mathbf{a}_t(r_k, \theta_k), \forall k \in \mathcal{K}, \quad (3)$$

where α_k , r_k , and θ_k denote the complex channel gain, the distance, and the angle of the user k , respectively. For target sensing, we assume that the self-interference has been well suppressed. Therefore, the TRM can be modeled as

$$\mathbf{G} = \alpha_s \mathbf{a}_r(r_s, \theta_s) \mathbf{a}_t^H(r_s, \theta_s), \quad (4)$$

where r_s and θ_s denote the distance and the direction of the sensing target, respectively.

Remark 1. According to (4), the TRM \mathbf{G} in the NF-ISAC system contains information regarding both distance and angle. Therefore, in contrast to far-field ISAC systems where only the angle can be estimated from \mathbf{G} , it is possible to carry out the joint distance and angle estimation in NF-ISAC systems.

Remark 2. According to (2), the information regarding distance and angle are contained in the terms $\varrho_t = \frac{(\delta_t^{(n)})^2}{2r}$ and $\vartheta_t = \delta_t^{(n)} \cos \theta$ (as well as the corresponding terms in $\mathbf{a}_r(r, \theta)$), respectively. Therefore, as the distance r increases, the value of ϱ_i can become negligible compared to the value of ϑ_i , which implies less information regarding distance in the TRM and thus leads to lower accuracy of distance estimation.

B. Communication Model

To carry out communication and sensing efficiently, the BS transmits the following joint communication and sensing signal at time n :

$$\mathbf{x}[n] = \mathbf{F}_{\text{RF}} \sum_{k \in \mathcal{K}} \mathbf{f}_{\text{BB},k} c_k[n] + \mathbf{F}_{\text{RF}} \mathbf{s}[n], \quad (5)$$

where $\mathbf{F}_{\text{RF}} \in \mathbb{C}^{N_t \times N_{\text{RF}}}$ denotes the analog precoder realized by the $N_t N_{\text{RF}}$ phase shifters, $\mathbf{f}_{\text{BB},k} \in \mathbb{C}^{N_{\text{RF}} \times 1}$ denotes the baseband digital beamformer for user k , $c_k[n] \in \mathbb{C}$ denote the normalized information symbol intended for user k , and $\mathbf{s}[n] \in \mathbb{C}^{N_{\text{RF}} \times 1}$ denotes the dedicated

sensing signal for achieving the full sensing degrees of freedom [3]. The information symbols and the dedicated sensing signal are assumed to be independently distributed. Thus, the covariance matrix of the transmit signal is given by

$$\mathbf{R}_x = \mathbf{F}_{\text{RF}} (\mathbf{F}_{\text{BB}} \mathbf{F}_{\text{BB}}^H + \mathbf{R}_s) \mathbf{F}_{\text{RF}}^H, \quad (6)$$

where $\mathbf{F}_{\text{BB}} = [\mathbf{f}_{\text{BB},1}, \dots, \mathbf{f}_{\text{BB},K}] \in \mathbb{C}^{N_{\text{RF}} \times K}$ denotes all digital baseband precoders for K communication users and $\mathbf{R}_s = \mathbb{E}[\mathbf{s}[n]\mathbf{s}[n]^H] \in \mathbb{C}^{N_{\text{RF}} \times N_{\text{RF}}}$ denotes the covariance matrix of the dedicated sensing signal with a general rank [3]. Then, the received signal at user k is given by

$$y_k[n] = \mathbf{h}_k^H \sum_{i \in \mathcal{K}} \mathbf{F}_{\text{RF}} \mathbf{f}_{\text{BB},i} c_i[n] + \mathbf{h}_k^H \mathbf{F}_{\text{RF}} \mathbf{s}[n] + z_k[n], \quad (7)$$

where $z_k[n] \sim \mathcal{CN}(0, \sigma_k^2)$ denotes the complex Gaussian noise with the power of σ_k^2 . Then, the SINR for decoding the desired signal at user k is given by

$$\gamma_k = \frac{|\mathbf{h}_k^H \mathbf{F}_{\text{RF}} \mathbf{f}_{\text{BB},k}|^2}{\sum_{i \neq k} |\mathbf{h}_k^H \mathbf{F}_{\text{RF}} \mathbf{f}_{\text{BB},i}|^2 + \mathbf{h}_k^H \mathbf{F}_{\text{RF}} \mathbf{R}_s \mathbf{F}_{\text{RF}}^H \mathbf{h}_k + \sigma_k^2}. \quad (8)$$

The corresponding communication throughput of the ISAC system is thus given by $R = \sum_{k \in \mathcal{K}} R_k = \sum_{k \in \mathcal{K}} \log_2(1 + \gamma_k)$.

C. Sensing Model and Proposed Estimation Scheme

Given the transmit signal in (5) and the target response matrix in (4), the received signal after the analog combination at the BS at time n is given by

$$\mathbf{y}_s[n] = \mathbf{W}_{\text{RF}} \mathbf{G} \mathbf{x}[n] + \mathbf{W}_{\text{RF}} \mathbf{z}_s[n], \quad (9)$$

where $\mathbf{W}_{\text{RF}} \in \mathbb{C}^{N_{\text{RF}} \times N_r}$ denotes the analog combination matrix at the BS and $\mathbf{z}_s[n] \sim \mathcal{CN}(0, \sigma_s^2 \mathbf{I}_N)$ denotes the complex Gaussian noise vector. The objective of sensing is to estimate the target parameters from the received echo signal samples over the whole coherent time block, i.e., $\mathbf{Y}_s = [\mathbf{y}_s[1], \dots, \mathbf{y}_s[T]]$. As suggested in [1], the analog combination \mathbf{W}_{RF} can be randomly selected from the unit circle for target sensing. Therefore, when the number of receive antennas is sufficiently large, it holds that $\frac{1}{N_r} \mathbf{W}_{\text{RF}} \mathbf{W}_{\text{RF}}^H \approx \mathbf{I}_{N_{\text{RF}}}$. As analyzed in **Remark 1**, the joint distance and angle estimation can be carried out with the near-field channel model. To this end, the concept of the classic Multiple Signal Classification (MUSIC) algorithm can be invoked, where the orthogonality between the signal subspaces is exploited. Based on the same idea, an

extended MUSIC algorithm is proposed for the joint distance and angle estimation is proposed as follows. Firstly, the covariance matrix of the received echo signal is given by

$$\mathbf{R}_{\mathbf{y}_s} = \underbrace{\mathbf{W}_{\text{RF}} \mathbf{G} \mathbf{R}_x \mathbf{G}^H \mathbf{W}_{\text{RF}}^H}_{\text{signal subspace}} + \underbrace{\sigma_s^2 N_r \mathbf{I}_{N_r}}_{\text{noise subspace}}. \quad (10)$$

It can be observed that the covariance matrix of the received signal consists of two orthogonal subspaces, namely signal subspace and noise subspace. In practice, the covariance matrix $\mathbf{R}_{\mathbf{y}_s}$ can be approximately obtained by averaging over the observations within a coherent time block, i.e., $\mathbf{R}_{\mathbf{y}_s} \approx \frac{1}{T} \sum_{n=1}^T \mathbf{y}_s[n] \mathbf{y}_s^H[n]$. With $\mathbf{R}_{\mathbf{y}_s}$ at hand, the signal subspace and the noise subspace can be estimated by the eigenvalue decomposition as follows:

$$\begin{aligned} \mathbf{R}_{\mathbf{y}_s} &= [\mathbf{E}_s, \mathbf{E}_n] \begin{bmatrix} \mathbf{D}_s & \\ & \mathbf{D}_n \end{bmatrix} [\mathbf{E}_s, \mathbf{E}_n]^H \\ &= \underbrace{\mathbf{E}_s \mathbf{D}_s \mathbf{E}_s^H}_{\text{signal subspace}} + \underbrace{\mathbf{E}_n \mathbf{D}_n \mathbf{E}_n^H}_{\text{noise subspace}}, \end{aligned} \quad (11)$$

where \mathbf{D}_s is the diagonal matrix with respect to the M largest eigenvalues with M denoting the number targets. In this work, we have $M = 1$. According to (10), the signal subspace is spanned by the vector $\tilde{\mathbf{a}}(r_s, \theta_s) = \mathbf{W}_{\text{RF}} \mathbf{a}(r_s, \theta_s)$. Therefore, by defining the projection operator onto the noise subspace as $\mathbf{P}_{\mathbf{E}_n} = \mathbf{E}_n (\mathbf{E}_n^H \mathbf{E}_n)^{-1} \mathbf{E}_n^H$, for any vector $\tilde{\mathbf{a}}(r, \theta)$, we have

$$\zeta(r, \theta) = \|\mathbf{P}_{\mathbf{E}_n} \tilde{\mathbf{a}}(r, \theta)\|^2 = \tilde{\mathbf{a}}^H(r, \theta) \mathbf{E}_n \mathbf{E}_n^H \tilde{\mathbf{a}}(r, \theta). \quad (12)$$

Based on the orthogonality between the signal subspace and the noise subspace, it holds that $\zeta(r, \theta) \rightarrow 0$ if and only if $r = r_s$ and $\theta = \theta_s$. Thus, the estimated distance and angle of the target are given by

$$(\hat{r}_s, \hat{\theta}_s) = \arg \min_{(r, \theta)} \zeta(r, \theta). \quad (13)$$

Typically, the mean square errors (MSE) between the estimated $(\hat{r}_s, \hat{\theta}_s)$ and the real (r_s, θ_s) is used to evaluate the sensing performance, i.e., $\epsilon_r^2 = \mathbb{E}[|r_s - \hat{r}_s|^2]$ and $\epsilon_\theta^2 = \mathbb{E}[|\theta_s - \hat{\theta}_s|^2]$. However, it is difficult to obtain the closed-form expression of the MSEs ϵ_r^2 and ϵ_θ^2 . As a remedy, we adopt the CRB as the performance matrix, which provides a lower bound of the MSE and has a closed-form expression. The CRBs on r_s and θ_s estimation are given as follows, respectively,

$$\text{CRB}_r = (J_{rr} - J_{r\theta}^2 J_{\theta\theta}^{-1})^{-1}, \text{CRB}_\theta = (J_{\theta\theta} - J_{r\theta}^2 J_{rr}^{-1})^{-1}, \quad (14)$$

where the exact expressions of J_{rr} , $J_{\theta\theta}$, and $J_{r\theta}$ and the derivation of the CRBs are given in Appendix A.

III. PROBLEM FORMULATION AND PROPOSED SOLUTION

A. Problem Formulation

Since the analog combination matrix \mathbf{W}_{RF} at the receiver can be randomly generated, we only focus on designing the analog beamformer and the digital baseband signals at the transmitter. It is worth noting that minimizing CRB_r and CRB_θ requires the same strategy, i.e., maximizing J_{rr} and $J_{\theta\theta}$ while minimizing $J_{r\theta}$. Therefore, in the following, we mainly consider the minimization of CRB_r . In particular, we aim to characterize the performance tradeoff between communication and sensing. The resulting optimization problem is given by

$$\max_{\Xi} \quad wR + (1 - w) \frac{\mu}{\text{CRB}_r}, \quad (15a)$$

$$\text{s.t.} \quad \text{tr}(\mathbf{R}_x) \leq P_t, \quad (15b)$$

$$|[\mathbf{F}_{\text{RF}}]_{i,j}| = 1, \forall i, j, \quad (15c)$$

where $\Xi = \{\mathbf{F}_{\text{RF}}, \mathbf{F}_{\text{BB}}, \mathbf{R}_s\}$ denotes the set of optimization variables, $w \in [0, 1]$ is the regularization factor that characterizes the priorities of communication and sensing performance, and $\mu > 0$ is to scale the value of $\frac{1}{\text{CRB}_r}$ to be comparable to R . However, the coupling of the analog beamformer \mathbf{F}_{RF} and the digital baseband signal $\{\mathbf{F}_{\text{BB}}, \mathbf{R}_s\}$ as well as the constant-modulus constraint make it difficult to obtain the globally optimal solution for Ξ .

B. Proposed Solution

In this subsection, we solve the optimization problem in (15). In particular, we define the fully-digital equivalent as $\tilde{\mathbf{F}} = \mathbf{F}_{\text{RF}}\mathbf{F}_{\text{BB}}$ and $\tilde{\mathbf{R}}_s = \mathbf{F}_{\text{RF}}\mathbf{R}_s\mathbf{F}_{\text{RF}}^H$. Then, the covariance matrix of the transmit signal can be rewritten as $\mathbf{R}_x = \tilde{\mathbf{F}}\tilde{\mathbf{F}}^H + \tilde{\mathbf{R}}_s$, and the communication SINR for user k can be rewritten as

$$\gamma_k(\tilde{\mathbf{F}}, \mathbf{R}_x) = \frac{|\mathbf{h}_k^H \tilde{\mathbf{f}}_k|^2}{\mathbf{h}_k^H \mathbf{R}_x \mathbf{h}_k - |\mathbf{h}_k^H \tilde{\mathbf{f}}_k|^2 + \sigma_k^2}, \quad (16)$$

where $\tilde{\mathbf{f}}_k$ is the vector at the k -th column of $\tilde{\mathbf{F}}$. In the proposed two-stage algorithm, we first obtain the high-quality solutions for $\tilde{\mathbf{F}}$ and $\tilde{\mathbf{R}}_s$ to problem (15). Then, \mathbf{F}_{RF} and $\{\mathbf{F}_{\text{BB}}, \mathbf{R}_s\}$ are designed to approximate the obtained $\tilde{\mathbf{F}}$ and $\tilde{\mathbf{R}}_s$. The details of the algorithm design are given as follows.

1) *Stage I*: Given the covariance matrix $\mathbf{R}_x = \tilde{\mathbf{F}}\tilde{\mathbf{F}}^H + \tilde{\mathbf{R}}_s$ and the SINR in (16), problem (15) can be recast as

$$\max_{t, \bar{\gamma}, \tilde{\mathbf{F}}, \mathbf{R}_x} w \sum_{k \in \mathcal{K}} \log_2(1 + \bar{\gamma}_k) + (1 - w)\mu t \quad (17a)$$

$$\text{s.t. } \gamma_k(\tilde{\mathbf{F}}, \mathbf{R}_x) \geq \bar{\gamma}_k, \forall k \in \mathcal{K}, \quad (17b)$$

$$\frac{1}{\text{CRB}_r} \geq t, \quad (17c)$$

$$\text{tr}(\mathbf{R}_x) \leq P_t, \quad (17d)$$

$$\mathbf{R}_x \succeq \mathbf{F}\mathbf{F}^H, \quad (17e)$$

where $\bar{\gamma} = [\bar{\gamma}_1, \dots, \bar{\gamma}_K]^T$ and t are auxiliary variables. Constraint (17e) stems from the fact that $\tilde{\mathbf{R}}_s \succeq 0$, which can be further transformed into the following linear matrix inequality according to the Schur complement condition:

$$(17e) \Leftrightarrow \begin{bmatrix} \mathbf{R}_x & \mathbf{F} \\ \mathbf{F}^H & \mathbf{I}_K \end{bmatrix} \succeq 0. \quad (18)$$

Similarly, by exploiting the Schur complement condition, the constraint (17c) can also be converted into the following linear matrix inequality:

$$(17c) \Leftrightarrow \begin{bmatrix} \text{tr}(\mathbf{Q}_{rr}\mathbf{R}_x) - t & \text{Re}(\text{tr}(\mathbf{Q}_{r\theta}\mathbf{R}_x)) \\ \text{Re}(\text{tr}(\mathbf{Q}_{r\theta}\mathbf{R}_x)) & \text{tr}(\mathbf{Q}_{\theta\theta}\mathbf{R}_x) \end{bmatrix} \succeq 0, \quad (19)$$

where $\mathbf{Q}_{ij} = \frac{2T}{\sigma_s^2 N_r} \dot{\mathbf{G}}_i^H \mathbf{W}_{\text{RF}}^H \mathbf{W}_{\text{RF}} \dot{\mathbf{G}}_j, \forall i, j \in \{r, \theta\}$. Therefore, the non-convexity of problem (17) only falls in the constraints (17b). To solve it, we introduce auxiliary variables $\bar{\omega} = [\bar{\omega}_1, \dots, \bar{\omega}_K]^T$, and then transform this constraint into the following equivalent form:

$$(17b) \Leftrightarrow \begin{cases} |\mathbf{h}_k^H \tilde{\mathbf{f}}_k|^2 \geq \bar{\omega}_k \bar{\gamma}_k \\ \mathbf{h}_k^H \mathbf{R}_x \mathbf{h}_k - |\mathbf{h}_k^H \tilde{\mathbf{f}}_k|^2 + \sigma_k^2 \leq \bar{\omega}_k \end{cases} \quad \forall k \in \mathcal{K}. \quad (20)$$

For the fixed β , the main obstacles to addressing the above two constraints stem from the quadratic terms $|\mathbf{h}_k^H \tilde{\mathbf{f}}_k|^2$ and the bilinear terms $\bar{\omega}_k \bar{\gamma}_k, \forall k \in \mathcal{K}$, which are intrinsically non-convex. In the following, we propose to solve them by invoking successive convex approximation (SCA).

We start with establishing the concave lower bound of $a(\tilde{\mathbf{f}}_k) = |\mathbf{h}_k^H \tilde{\mathbf{f}}_k|^2$. Given $\tilde{\mathbf{f}}^{[t]}$ obtained in the t -th iteration and the convexity of $a(\tilde{\mathbf{f}}_k)$, the following affine lower bound of it can be

obtained through the first-order Taylor expansion:

$$\underline{a}^{[t]}(\tilde{\mathbf{f}}_k) = -(\tilde{\mathbf{f}}_k^{[t]})^H \mathbf{h}_k \mathbf{h}_k^H \tilde{\mathbf{f}}_k^{[t]} + 2\text{Re} \left\{ \tilde{\mathbf{f}}_k^H \mathbf{h}_k \mathbf{h}_k^H \tilde{\mathbf{f}}_k^{[t]} \right\}. \quad (21)$$

Next, for the bilinear function, we have $\phi(\bar{\omega}_k, \bar{\gamma}_k) = \bar{\omega}_k \bar{\gamma}_k = \frac{1}{4}((\bar{\omega}_k + \bar{\gamma}_k)^2 - (\bar{\omega}_k - \bar{\gamma}_k)^2)$. Therefore, given $\bar{\omega}_k^{[t]}$ and $\bar{\gamma}_k^{[t]}$, the following convex upper bound $\bar{\phi}^{[t]}(x, y)$ can be readily obtained by the first-order Taylor expansion:

$$\bar{\phi}^{[t]}(\bar{\omega}_k, \bar{\gamma}_k) = \frac{1}{4}(\bar{\omega}_k + \bar{\gamma}_k)^2 - \frac{1}{4} \left(-(\bar{\omega}_k^{[t]} - \bar{\gamma}_k^{[t]})^2 + 2(\bar{\omega}_k^{[t]} - \bar{\gamma}_k^{[t]})(\bar{\omega}_k - \bar{\gamma}_k) \right), \quad (22)$$

Consequently, problem (17) can be approximated by

$$\max_{\substack{t, \bar{\gamma}, \bar{\omega}, \\ \tilde{\mathbf{F}}, \mathbf{R}_x}} \sum_{k \in \mathcal{K}} \log_2(1 + \bar{\gamma}_k) + (1 - w)\mu t \quad (23a)$$

$$\text{s.t.} \quad \underline{a}^{[t]}(\tilde{\mathbf{f}}_k) \geq \bar{\phi}^{[t]}(\bar{\omega}_k, \bar{\gamma}_k), \forall k \in \mathcal{K}, \quad (23b)$$

$$\mathbf{h}_k^H \mathbf{R}_x \mathbf{h}_k - \underline{a}^{[t]}(\tilde{\mathbf{f}}_k) + \sigma_k^2 \leq \bar{\omega}_k, \forall k \in \mathcal{K}, \quad (23c)$$

$$(17d), (18), (19). \quad (23d)$$

The above problem is convex and can be effectively solved by the standard interior-point algorithm. After obtaining the solution $\tilde{\mathbf{F}}^d$ and \mathbf{R}_x^d for the fully-digital communication beamformers and transmit covariance matrix via SCA, the solution for the covariance matrix of the dedicated sensing signal can be obtained by $\tilde{\mathbf{R}}_s^d = \mathbf{R}_x^d - \tilde{\mathbf{F}}^d(\tilde{\mathbf{F}}^d)^H$.

2) *Stage II*: In this stage, we optimize \mathbf{F}_{RF} and $\{\mathbf{F}_{\text{BB}}, \mathbf{R}_s\}$ to approximate the solution $\tilde{\mathbf{F}}^d$ and $\tilde{\mathbf{R}}_s^d$ obtained at Stage I. In particular, we aim to minimize the distance between them characterized by the Frobenius norm, i.e., $\|\mathbf{F}_{\text{RF}}\mathbf{F}_{\text{BB}} - \tilde{\mathbf{F}}^d\|_F^2$ and $\|\mathbf{F}_{\text{RF}}\mathbf{R}_s\mathbf{F}_{\text{RF}}^H - \tilde{\mathbf{R}}_s^d\|_F^2$. It can be observed that the former is in a standard quadratic form while the latter is not. To simplify the optimization of the latter, we first decompose the matrix $\tilde{\mathbf{R}}_s$ via the eigenvalue decomposition, i.e., $\tilde{\mathbf{R}}_s = \sum_{i=1}^Q \tilde{\mathbf{v}}_i^d (\tilde{\mathbf{v}}_i^d)^H$, where $\tilde{\mathbf{v}}_i, \forall i$, are the orthogonal vectors consisting of the eigenvalue and the corresponding eigenvector, and Q denotes the rank of the matrix $\tilde{\mathbf{R}}_s^d$. Following this, we rewrite the matrix \mathbf{R}_s as $\mathbf{R}_s = \sum_{i=1}^Q \mathbf{v}_i \mathbf{v}_i^H$. Then, the minimization of $\|\mathbf{F}_{\text{RF}}\mathbf{R}_s\mathbf{F}_{\text{RF}}^H - \tilde{\mathbf{R}}_s^d\|_F^2$ can be achieved by minimizing $\sum_{i=1}^Q \|\mathbf{F}_{\text{RF}}\mathbf{v}_i - \tilde{\mathbf{v}}_i^d\|_2^2 = \|\mathbf{F}_{\text{RF}}\mathbf{V} - \tilde{\mathbf{V}}^d\|_F^2$, where $\mathbf{V} = [\mathbf{v}_1, \dots, \mathbf{v}_Q]$

Algorithm 1 Two-stage algorithm for solving problem (15)

- 1: **Stage I:**
 - 2: initialize feasible $\tilde{\mathbf{F}}^{[0]}$ and $\mathbf{R}_x^{[0]}$, and set $t = 0$.
 - 3: **repeat**
 - 4: update $\tilde{\mathbf{F}}^{[t+1]}$ and $\mathbf{R}_x^{[t+1]}$ by solving problem (23).
 - 5: $t = t + 1$.
 - 6: **until** the fractional reduction of the objective value of problem (17) falls below a predefined threshold.
 - 7: set $\tilde{\mathbf{F}}^d = \tilde{\mathbf{F}}^{[t]}$ and $\tilde{\mathbf{R}}_s^d = \mathbf{R}_x^{[t]} - \tilde{\mathbf{F}}^d(\tilde{\mathbf{F}}^d)^H$
 - 8: **Stage II:**
 - 9: initialize feasible $\mathbf{F}_{\text{RF}}^{[0]}$, obtain $\tilde{\mathbf{V}}^d$ via the eigenvalue decomposition of $\tilde{\mathbf{R}}_s^d$, and set $t = 0$.
 - 10: **repeat**
 - 11: update $\mathbf{F}_{\text{BB}}^{[t+1]} = (\mathbf{F}_{\text{RF}}^{[t]})^\dagger \tilde{\mathbf{F}}^d$ and $\mathbf{V}^{[t+1]} = (\mathbf{F}_{\text{RF}}^{[t]})^\dagger \tilde{\mathbf{V}}^d$.
 - 12: update $\mathbf{F}_{\text{RF}}^{[t+1]}$ via the BCD method in [8].
 - 13: $t = t + 1$.
 - 14: **until** the fractional reduction of the objective value of problem (24) falls below a predefined threshold.
 - 15: normalize the final solution to satisfy the power constraint.
-

and $\tilde{\mathbf{V}}^d = [\tilde{\mathbf{v}}_1^d, \dots, \tilde{\mathbf{v}}_Q^d]$. Then, the resulting optimization problem is given as follows:

$$\max_{\mathbf{F}_{\text{RF}}, \mathbf{F}_{\text{BB}}, \mathbf{V}} \|\mathbf{F}_{\text{RF}} \mathbf{F}_{\text{BB}} - \tilde{\mathbf{F}}^d\|_F^2 + \|\mathbf{F}_{\text{RF}} \mathbf{V} - \tilde{\mathbf{V}}^d\|_F^2, \quad (24a)$$

$$\text{s.t.} \quad |[\mathbf{F}_{\text{RF}}]_{i,j}| = 1, \forall i, j, \quad (24b)$$

Here, the power constraint is temporarily removed to simplify the optimization. The above algorithm can be solved by optimizing \mathbf{F}_{RF} and $\{\mathbf{F}_{\text{BB}}, \mathbf{V}\}$ alternately. For the fixed \mathbf{F}_{RF} , the closed-form optimal solutions for \mathbf{F}_{BB} and \mathbf{V} can be readily obtained by the least-square solution as $\mathbf{F}_{\text{BB}} = \mathbf{F}_{\text{RF}}^\dagger \tilde{\mathbf{F}}^d$ and $\mathbf{V} = \mathbf{F}_{\text{RF}}^\dagger \tilde{\mathbf{V}}^d$. Then, for the fixed $\{\mathbf{F}_{\text{BB}}, \mathbf{V}\}$, a stationary point of problem (24) with respect to \mathbf{F}_{RF} can be obtained by the low-complexity block coordinate descent (BCD) method. The detail of the BCD method can be found in [8, Appendix B] and is thus omitted here. Denote $\bar{\mathbf{F}}_{\text{RF}}$ and $\{\bar{\mathbf{F}}_{\text{BB}}, \bar{\mathbf{V}}\}$ as the obtained solution to problem (24). Then, $\{\bar{\mathbf{F}}_{\text{BB}}, \bar{\mathbf{V}}\}$ are normalized to satisfy the power constraint, resulting in the following final solutions $\mathbf{F}_{\text{BB}}^* = \sqrt{\lambda} \bar{\mathbf{F}}_{\text{BB}}$ and $\mathbf{V}^* = \sqrt{\lambda} \bar{\mathbf{V}}$, where $\lambda = \frac{P_t}{\|\bar{\mathbf{F}}_{\text{RF}} \bar{\mathbf{F}}_{\text{BB}}\|_F^2 + \|\bar{\mathbf{F}}_{\text{RF}} \bar{\mathbf{V}}\|_F^2}$ is the power scaling factor.

The proposed two-stage algorithm for solving problem (15) is summarized in **Algorithm 1**. The complexity of the proposed algorithm is analyzed as follows. Firstly, the main complexity in Stage I arises from solving problem (23) with $p = 2(K + 1) + N_t K + N_t^2$ optimization variables, whose complexity is mainly determined by the K SOC constraints (23b) with a dimension of

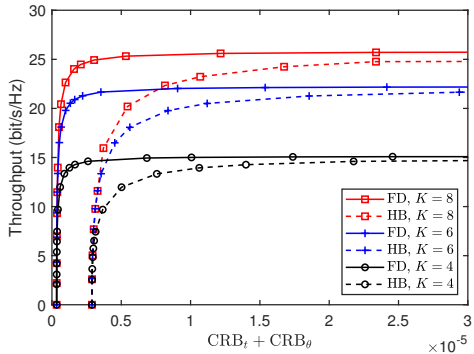


Fig. 2: Performance tradeoff between communication and sensing.

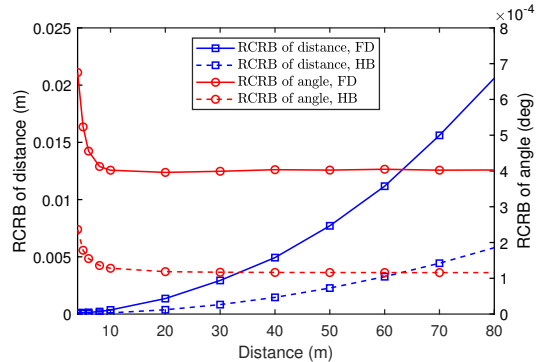


Fig. 3: RCRB versus distance r_s .

$N_t + 2$ and the semidefinite constraint (18) with a dimension of $(N_t + K) \times (N_t + K)$. Therefore, the complexity of each iteration in Stage I is given by $\mathcal{O}(p(p^2 + K + K(N_t + 2)^2 + p(N_t + K)^2 + (N_t + K)^3))$ [9]. Furthermore, for each iteration in Stage II, the complexity mainly arises from the BCD method, whose complexity is $\mathcal{O}(I_{bcd}N_t^2N_{\text{RF}}^2)$ with I_{bcd} denoting the number of iterations of BCD [8].

IV. NUMERICAL RESULTS

In this section, numerical results are provided to verify the effectiveness of the proposed NF-ISAC framework. Here, we assume a BS with $N_t = N_r = 128$ antennas connected to $N_{\text{RF}} = 12$ RF chains, with a carrier frequency of $f = 10$ GHz ($\lambda = 3$ cm). The antenna spacing is set to $d = \frac{\lambda}{2}$ and the half distance between the transmit and receive antenna arrays is set to $D = 2d$. The pathloss exponent is set to 2.2. The location of the sensing target is assumed to be $r_s = 10$ m and $\theta_s = 110^\circ$, and communication users are randomly located within the range of $0 \sim 15$ m. Moreover, the maximum transmit power is set to $P_t = -13$ dBm, and the noise power is set to $\sigma_k^2 = \sigma_s^2 = -73$ dBm. For comparison, we exploit the fully-digital (FD) system as the benchmark, where each antenna at the BS is connected to a dedicated RF chain.

A. Performance Tradeoff

In Fig. 2, we investigate the performance tradeoff between communication and sensing, considering different numbers of communication users. As can be observed, the optimal performance of communication and sensing cannot be achieved simultaneously. This is because communication and sensing require the power emitted from the BS to focus on different locations. Furthermore,

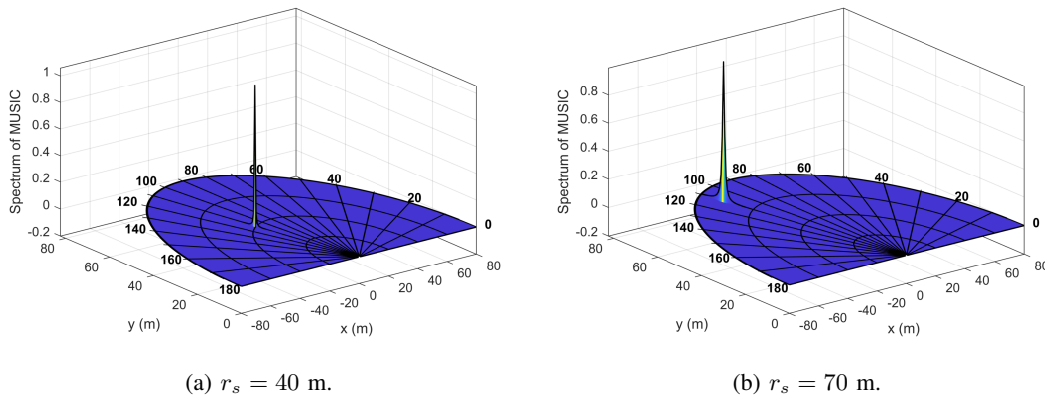


Fig. 4: Spectrum of MUSIC with different distances.

compared with FD systems, both communication throughput and sensing accuracy are reduced in HB systems. In particular, the performance loss of communication happens at the transmitter, where fewer RF chains cannot achieve the optimal multiplexing gain. On the contrary, for target sensing, the performance loss is mainly caused by the HB structure at the receiver, which significantly reduces the dimension of signal samples.

B. Root CRB versus Distance

In Fig. 3, we study the impact of the distance of the target on the distance and angle estimation, where we fix the sensing SNR to 10 dB for a fair comparison. It can be observed that as the distance r_s becomes larger, the root CRB (RCRB) of distance gradually increases, which implies lower accuracy of distance estimation. Such a result is consistent with our analysis in **Remark 2**. In addition, it is interesting to see that the RCRB of angle is firstly reduced slightly and then keeps almost unchanged. This is also expected because as r_s increases, the near-field channel degrades to the far-field channel. In this case, the echo signal at each antenna comes from almost the same direction, which is preferred by the angle estimation. However, compared with the reduction of the distance accuracy due to the farther target (with RCRB from 4×10^{-5} m to 2×10^{-2} m), the reduction of the angle accuracy in the near region (with RCRB from 4×10^{-4} degree to 7×10^{-4} degree) is negligible.

C. Spectrum of MUSIC

In Fig. 4, we demonstrate the spectrum of the extended MUSIC algorithm, i.e., $1/\zeta(r, \theta)$, over a fine grid of $r \in [0, 80]$ m and $\theta \in [0^\circ, 180^\circ]$. It can be seen that the largest response in the

spectrum occurs around the real locations of the sensing target, which confirm the effectiveness of the proposed framework. Furthermore, for both cases of $r_s = 40$ m and $r_s = 70$ m, very high accuracy can be achieved for angle estimation. However, compared with the case of $r_s = 40$ m, the high-value region of the spectrum becomes wider along the distance axis when $r_s = 70$ m, which indicates a lower accuracy of distance estimation and thus also consistent with **Remark 2**.

V. CONCLUSION

A NF-ISAC framework has been proposed, where the communication and sensing functions are carried out simultaneously based on the spherical-wave-based near-field channel model. The joint distance and angle estimation of the target was achieved in the NF-ISAC framework. The tradeoff between communication and sensing performance was characterized. It is suggested that the ISAC can benefit more from the near-field compared with the far-field. Therefore, some methods, such as redesigning the antenna shape, can be exploited in future works to enlarge the near-field region.

APPENDIX A: DERIVATION OF CRBS

The CRB can be calculated by the inverse of the Fisher information matrix (FIM). According to [10, Appendix 3C], the FIM with respect to estimating r_s and θ_s from \mathbf{Y}_s is

$$\mathbf{J} = \begin{bmatrix} J_{rr} & J_{r\theta} \\ J_{r\theta} & J_{\theta\theta} \end{bmatrix}, \quad (25)$$

where $J_{ij} = \frac{2T}{\sigma_s^2 N_r} \text{Re} \left\{ \text{tr} \left(\mathbf{W}_{\text{RF}} \dot{\mathbf{G}}_i \mathbf{R}_x \dot{\mathbf{G}}_j^H \mathbf{W}_{\text{RF}}^H \right) \right\}$, $\forall i, j \in \{r, \theta\}$, and $\dot{\mathbf{G}}_r = \alpha_s \left(\frac{\partial \mathbf{a}_r}{\partial r_s} \mathbf{a}_t^H + \mathbf{a}_r \frac{\partial \mathbf{a}_t^H}{\partial r_s} \right)$ and $\dot{\mathbf{G}}_\theta = \alpha_s \left(\frac{\partial \mathbf{a}_r}{\partial \theta_s} \mathbf{a}_t^H + \mathbf{a}_r \frac{\partial \mathbf{a}_t^H}{\partial \theta_s} \right)$ denote the derivatives of \mathbf{G} with respect to r_s and θ_s , respectively. In particular, we have $\left[\frac{\partial \mathbf{a}_i}{\partial r_s} \right]_n = \frac{j\pi(\delta_i^{(n)})^2}{\lambda r_s^2} \psi_i^{(n)}$ and $\left[\frac{\partial \mathbf{a}_i}{\partial \theta_s} \right]_n = \frac{-j2\pi\delta_i^{(n)} \sin(\theta_s)}{\lambda} \psi_i^{(n)}$, where $\psi_i^{(n)} = \left(-\delta_i^{(n)} \cos \theta_s + \frac{(\delta_i^{(n)})^2}{2r_s} \right) [\mathbf{a}_i]_n$, $\forall i \in \{t, r\}$. Then, the corresponding CRB matrix is given by

$$\text{CRB} = \mathbf{J}^{-1} = \frac{1}{J_{rr}J_{\theta\theta} - J_{r\theta}^2} \begin{bmatrix} J_{\theta\theta} & -J_{r\theta} \\ -J_{r\theta} & J_{rr} \end{bmatrix}. \quad (26)$$

The diagonal elements of the CRB matrix represent lower bounds of MSEs regarding the estimation of r_s and θ_s , respectively. Therefore, the expressions in (14) can be obtained.

REFERENCES

- [1] F. Liu *et al.*, “Joint radar and communication design: Applications, state-of-the-art, and the road ahead,” *IEEE Trans. Commun.*, vol. 68, no. 6, pp. 3834–3862, Jun. 2020.
- [2] X. Mu, Z. Wang, and Y. Liu, “NOMA for integrating sensing and communications towards 6G: A multiple access perspective,” *IEEE Wireless Commun.*, early access, Jan. 2023, doi:10.1109/MWC.015.2200559.
- [3] X. Liu, T. Huang, N. Shlezinger, Y. Liu, J. Zhou, and Y. C. Eldar, “Joint transmit beamforming for multiuser MIMO communications and MIMO radar,” *IEEE Trans. Signal Process.*, vol. 68, pp. 3929–3944, Jun. 2020.
- [4] F. Liu, Y.-F. Liu, A. Li, C. Masouros, and Y. C. Eldar, “Cramér-rao bound optimization for joint radar-communication beamforming,” *IEEE Trans. Signal Process.*, vol. 70, pp. 240–253, Dec. 2021.
- [5] Z. Wang, Y. Liu, X. Mu, Z. Ding, and O. A. Dobre, “NOMA empowered integrated sensing and communication,” *IEEE Commun. Lett.*, vol. 26, no. 3, pp. 677–681, Mar. 2022.
- [6] E. Björnson *et al.*, “Massive MIMO is a reality—What is next?: Five promising research directions for antenna arrays,” *Digital Signal Process.*, vol. 94, pp. 3–20, Nov. 2019.
- [7] J. Sherman, “Properties of focused apertures in the Fresnel region,” *IRE Trans. on Antennas Propag.*, vol. 10, no. 4, pp. 399–408, Jul. 1962.
- [8] Q. Shi and M. Hong, “Spectral efficiency optimization for millimeter wave multiuser MIMO systems,” *IEEE J. Sel. Topics Signal Process.*, vol. 12, no. 3, pp. 455–468, Jun. 2018.
- [9] A. Ben-Tal and A. Nemirovski, *Lectures on modern convex optimization: analysis, algorithms, and engineering applications*, Philadelphia, PA, USA: SIAM, 2001.
- [10] S. M. Kay, *Fundamentals of statistical signal processing: estimation theory*. Englewood Cliffs, NJ: Prentice-Hall, 1993.